Lipid domain–dependent regulation of single-cell wound repair

Emily M. Vaughan[a,b], Jae-Sung You[a,c], Hoi-Ying Elsie Yu[a,b], Amber Lasek[b], Nicolas Vitale[d], Troy A. Hornberger[a,c], and William M. Bement[a,b,e]

[a]Program in Cellular and Molecular Biology, [b]Department of Zoology, [c]Department of Comparative Biosciences, and [e]Laboratory of Cell and Molecular Biology, University of Wisconsin–Madison, Madison, WI 53706; [d]Institut des Neurosciences Cellulaires et Integratives, Centre National de la Recherche Scientifique UPR 3212, and Université de Strasbourg, 67400 Strasbourg, France

ABSTRACT **After damage, cells reseal their plasma membrane and repair the underlying cortical cytoskeleton. Although many different proteins have been implicated in cell repair, the potential role of specific lipids has not been explored. Here we report that cell damage elicits rapid formation of spatially organized lipid domains around the damage site, with different lipids concentrated in different domains as a result of both de novo synthesis and transport. One of these lipids—diacylglycerol (DAG)—rapidly accumulates in a broad domain that overlaps the zones of active Rho and Cdc42, GTPases that regulate repair of the cortical cytoskeleton. Formation of the DAG domain is required for Cdc42 and Rho activation and healing. Two DAG targets, protein kinase C (PKC) β and η, are recruited to cell wounds and play mutually antagonistic roles in the healing process: PKCβ participates in Rho and Cdc42 activation, whereas PKCη inhibits Rho and Cdc42 activation. The results reveal an unexpected diversity in subcellular lipid domains and the importance of such domains for a basic cellular process.**

Monitoring Editor
David G. Drubin
University of California, Berkeley

Received: Mar 27, 2014
Revised: Apr 14, 2014
Accepted: Apr 21, 2014

INTRODUCTION

One of the most fascinating and important features of eukaryotic cells is their ability to rapidly polarize in response to intrinsic or extrinsic signals. This polarization is often first manifest at the plasma membrane, where different proteins are recruited as cells are exposed to local stimuli such as growth factors, cell–cell contact, or progression through the cell cycle. Such polarization is universal and underlies an enormous number of fundamental biological processes (Mellman and Nelson, 2008).

Cell damage represents a local stimulus, the response to which is both conserved and essential (Sonnemann and Bement, 2011). Cell repair results from two complementary processes: resealing of the plasma membrane (McNeil and Steinhardt, 2003) and restitution of the cortical cytoskeleton (Sonnemann and Bement, 2011). The importance of these processes is considerable, in that excessive cell damage and/or compromised repair results in or is associated with a variety of pathologies, including the muscular dystrophies (Laval and Bushby, 2004), acute lung injury (Godin *et al.*, 2011), and diabetes (Howard *et al.*, 2011).

Efforts to understand the cell damage–repair cycle have focused on proteins, resulting in the identification of several players that are needed to either limit cell damage in response to normal physical stresses exerted on the plasma membrane, such as dystrophin (Lapidos *et al.*, 2004), or participate in the repair process, such as dysferlin (Bansal *et al.*, 2003), annexin (Lennon *et al.*, 2003; McNeil *et al.*, 2006), and MG53 (Cai *et al.*, 2009). Several proteins have also been implicated in cortical cytoskeleton repair, including the Rho GTPases Rho, Cdc42, and Rac (Benink and Bement, 2005; Abreu-Blanco *et al.*, 2014), the actin regulatory protein cortactin (Godin *et al.*, 2011), Abr, a guanine nucleotide exchange factor (GEF) and GTPase-activating protein for Rho GTPases (Vaughan *et al.*, 2011), and E-cadherin (Abreu-Blanco *et al.*, 2011). However, the potential role of specific lipids in cell repair has not been systematically explored, in spite of the fact that lipid domains participate in other polarization events (e.g., Takeda *et al.*, 2004; Liu *et al.*, 2009),

This article was published online ahead of print in MBoC in Press (http://www.molbiolcell.org/cgi/doi/10.1091/mbc.E14-03-0839) on April 30, 2014.

Address correspondence to: William M. Bement (wmbement@wisc.edu).

Abbreviations used: DAG, diacylglycerol; GAP, GTPase-activating protein; GEF, guaninenucleotide exchange factor; PA, phosphatidic acid; PIP2, phosphatidylinositol 4,5 bisphosphate; PIP3, phosphatidylinositol 3,4,5 bisphosphate; PKC, protein kinase C; PLC, phospholipase C; PS, phosphatidylserine.

many of the known protein players in cell repair bind lipids, and plasma membrane damage necessarily entails local disruption of the lipid environment. Here we analyze the potential role of different lipids in single-cell repair in the *Xenopus* oocyte model. We find that plasma membrane damage elicits profound local changes in the abundance and distribution of different phospholipids, different lipids sort into overlapping but spatially distinct domains around wounds, and at least one of the lipids studied, diacylglycerol, is essential for proper wound repair.

RESULTS

Multiple lipid domains form around single-cell wounds

To explore the potential role of lipids in the repair process, we microinjected *Xenopus* oocytes with mRNAs encoding probes for different lipids and a probe for active Cdc42 (monomeric red fluorescent protein [mRFP]-wGBD; Figure 1, A′–E′) to serve as a spatial reference point, since active Cdc42 consistently localizes to a zone ~5 μm from the wound edge (Benink and Bement, 2005). The distribution of different lipids was compared using previously described probes: phosphatidic acid (PA) was detected with a fragment of Spo20p (Zeniou-Meyer *et al.*, 2007); diacylglycerol (DAG) was detected with the C1 domain of protein kinase C (PKC) η (Dries *et al.*, 2007; Yu and Bement, 2007); phosphatidylinositol 3,4,5-trisphosphate (PIP3) was detected by GRP1 PH (Gray *et al.*, 1999); phosphatidylinositol 4,5-bisphosphate (PIP2) was detected by phospholipase C (PLC) δ PH (Raucher *et al.*, 2000); and phosphatidylserine (PS) was detected by the C2 domain of lactadherin (Yeung *et al.*, 2008). Because the PA and DAG probes are less well characterized than those for PIP2, PIP3, and PS, the specificity of these probes was tested by analyzing localization of point mutants lacking either PA- or DAG-binding ability, respectively; such point mutants failed to localize to wounds (Supplemental Figure S1, B and C). To further ensure the specificity of the results, the distribution of farnesylated GFP (fGFP)—a generic marker for plasma membrane proteins—was followed.

Cells expressing mRFP-wGBD and the various lipid probes were wounded and analyzed by four-dimensional imaging to track patterns of lipid distribution over time. Although each lipid ultimately showed a distinct spatiotemporal distribution pattern (see later discussion), the probes revealed two general patterns of lipid behavior based on kinetics: slow, in which the probes did not reveal changes in lipid distribution until after formation of the Cdc42 zone (~20–40 s postwounding), and fast, in which the probes revealed changes in lipid distribution before or coincident with the formation of Cdc42 zone (~15–20 s postwounding; Figures 1 and 2A). Slow behavior was displayed by PIP3, PIP2, and PS. PIP3 and PS concentrated just inside the active Cdc42 zone, whereas PIP2 concentrated outside the Cdc42 zone (Figure 1, A–A′, B–B′, and C–C′). fGFP also accumulated around wounds, in a region that overlapped the Cdc42 zone; however, this was a relatively late event, and the extent of accumulation was relatively modest (Supplemental Figure S1, A–A′). Fast behavior was displayed by PA and DAG. PA showed the fastest change, undergoing depletion around wounds immediately after wounding (i.e., within 6 s) and then reaccumulating and concentrating predominantly inside the nascent Cdc42 zone (Figure 1, D–D′). DAG also concentrated predominantly inside the forming Cdc42 zone but without undergoing an initial depletion around wounds (Figure 1, E–E′).

The apparent differences in distribution of the various lipid probes relative to active Cdc42 indicated a surprising degree of lipid domain diversity around wounds. This notion was further supported by experiments in which the dynamic distributions of different lipid probes were directly compared with each other. For example, the DAG and PIP3 domains were circumscribed by the PIP2 domain (Figure 1, F and G), as expected based on their positions relative to Cdc42. However, other comparisons suggested even more compartmentalization. For example, PS and PA, both of which concentrate inside the Cdc42 zone, nevertheless display overlapping but distinct domains, with the peak of PA signal just outside the peak of the PS signal (Figure 1H). In other words, the region immediately next to the wound has at least two overlapping but also distinct domains with qualitatively different lipid compositions, and these are different again from the region farther from the wound edge, which is enriched in PIP2. Similarly, triple labeling using fluorescent actin and different pairs of lipid probes reveals the existence of at least three overlapping but distinct compartments (Supplemental Figure S1D). Finally, even lipids that show a similar distribution at 90 s, such as DAG and PA (Figure 1I), behave differently at earlier time points (Figure 1, D and E), indicating a considerable degree of plasma membrane lipid compartmentalization.

PA and DAG are generated at the wound edge coincident with Rho GTPase activation

DAG and PA were the lipids most rapidly and extensively concentrated at wound edges (Figures 1 and 2, A and B), as might be expected if these lipids serve as upstream regulators of Rho and Cdc42. Consistent with this possibility, direct comparison of the recruitment patterns of DAG and PA to active Rho indicated that these two lipids are recruited at the same time and in the same place as Rho activation (Figure 2, C–C′ and D–D′). Because Rho and Cdc42 are activated before and independently of actomyosin-powered cortical flow after wounding (Benink and Bement, 2005), and as a means to distinguish between lipid accumulation at wounds via transport versus de novo synthesis, we assessed the relationship between the different lipids and cortical flow. Brightest-point projections demonstrated that PIP3, PIP2, and PS undergo extensive cortical flow toward the wounds, whereas PA and DAG display relatively little cortical flow (Figure 2E), consistent with accumulation via de novo generation rather than transport. Further, pretreatment of cells with latrunculin A before wounding to disrupt cortical F-actin and block cortical flow failed to prevent accumulation of DAG and PA at wounds (Figure 2F), whereas this same treatment disrupted normal patterns of accumulation of the other lipids (unpublished data). These results are consistent with PA and DAG acting upstream of Rho and Cdc42 and show that these lipids accumulate around wounds at least in part due to wound-triggered de novo synthesis.

DAG generation occurs via the phosphatidylcholine-PLC/sphingomyelin synthase pathway, whereas PA is generated via phospholipase D and DAG kinase

On the basis of the foregoing results, we assessed the potential sources of the fast lipids—PA and DAG. Because a given lipid is typically the output of several different pathways, and because, conversely, a given lipid can serve as a precursor for several other different lipids, we used pharmacological approaches (Figure 3H). DAG is generated from PA via phospholipase D (PLD) and phosphatidic acid phosphohydrolase (PAPH), from phosphatidylinositol 4,5-bisphosphate via PIP2-PLC, from ceramide/phosphatidylcholine (PC) via sphingomyelin synthase (SMS), and from PC via PC-PLC (Wakelam, 1998). To determine whether PA was a source of DAG, we treated cells with 5-fluoro-2-indolyl des-chlorohalopemide (FIPI), a highly specific PLD inhibitor (Su *et al.*, 2009). FIPI did not change DAG levels after wounding (Figure 3, B and B′), but it significantly reduced PA levels (Figure 3, E and E′), as determined by quantifying

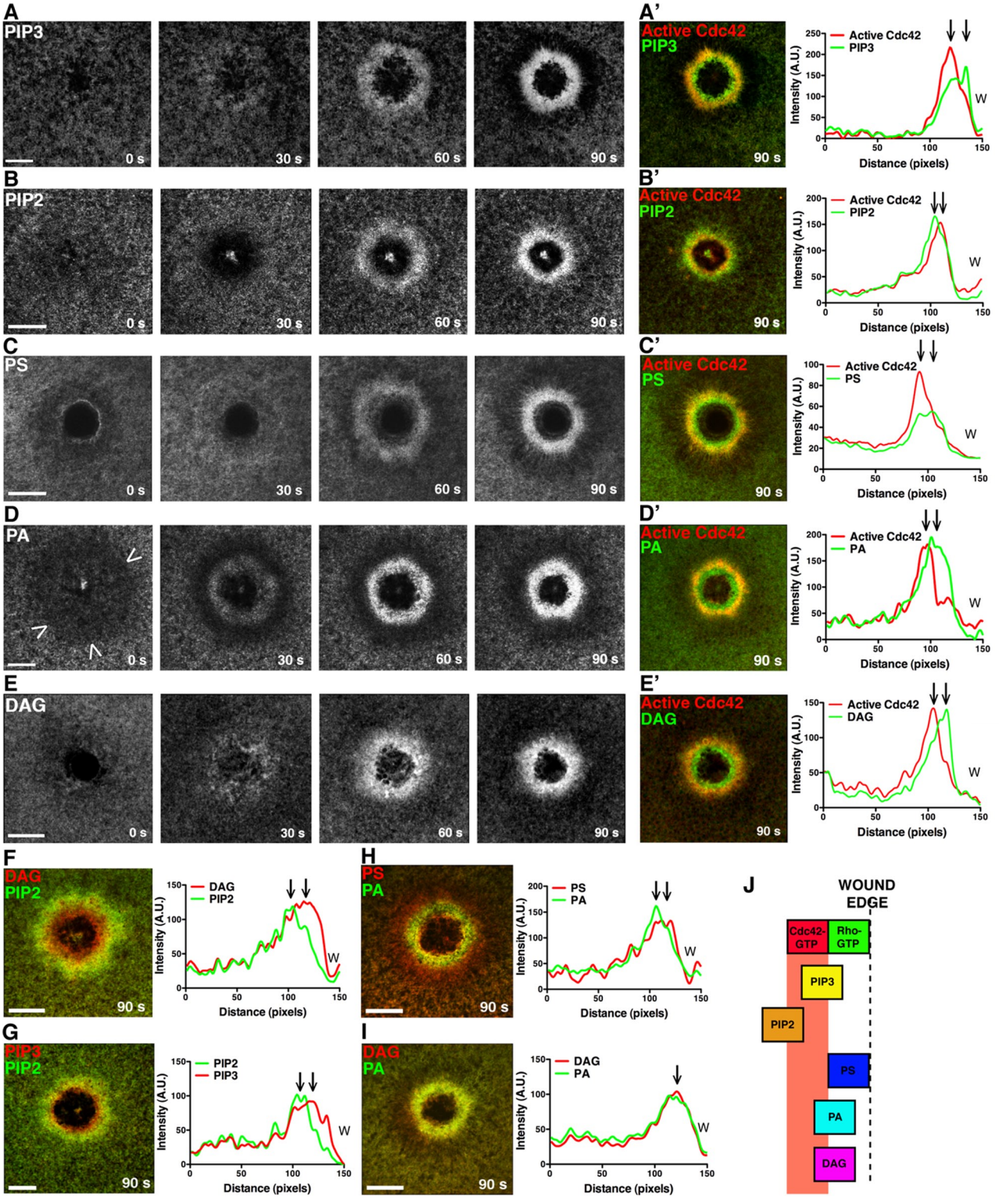

FIGURE 1: Multiple, distinct lipid domains form around single-cell wounds. (A) eGFP-PH (GRP1) detects PIP3 accumulation. (A′) PIP3 peak enrichment occurs inside the active Cdc42 zone at 90 s. (B) eGFP-PH (PLCδ) detects PIP2 enrichment. (B′) PIP2 peak enrichment is outside the active Cdc42 zone at 90 s. (C) eGFP-C2 (lactadherin) detects PS enrichment. (C′) PS peak enrichment occurs inside the active Cdc42 zone at 90 s. (D) eGFP-Spo20 detects a region of PA depletion (arrowheads) immediately after wounding, followed by enrichment. (D′) The peak of PA signal is found inside the zone of active Cdc42 at 90 s. (E) eGFP-C1 (PKCη) detects a region of DAG enrichment. (E′) The peak of DAG enrichment leads the peak of active Cdc42 at 90 s. (F) The peak of DAG enrichment leads the peak of PIP2. (G) The peak of PIP3 enrichment leads the peak of PIP2. (H) The peak PS signal leads the peak PA signal. (I) The peak DAG and PA signal are colocalized. (J) Schematic of lipid localization relative to the active Rho and Cdc42 zones. Scale bar, 20 μm. W, wound.

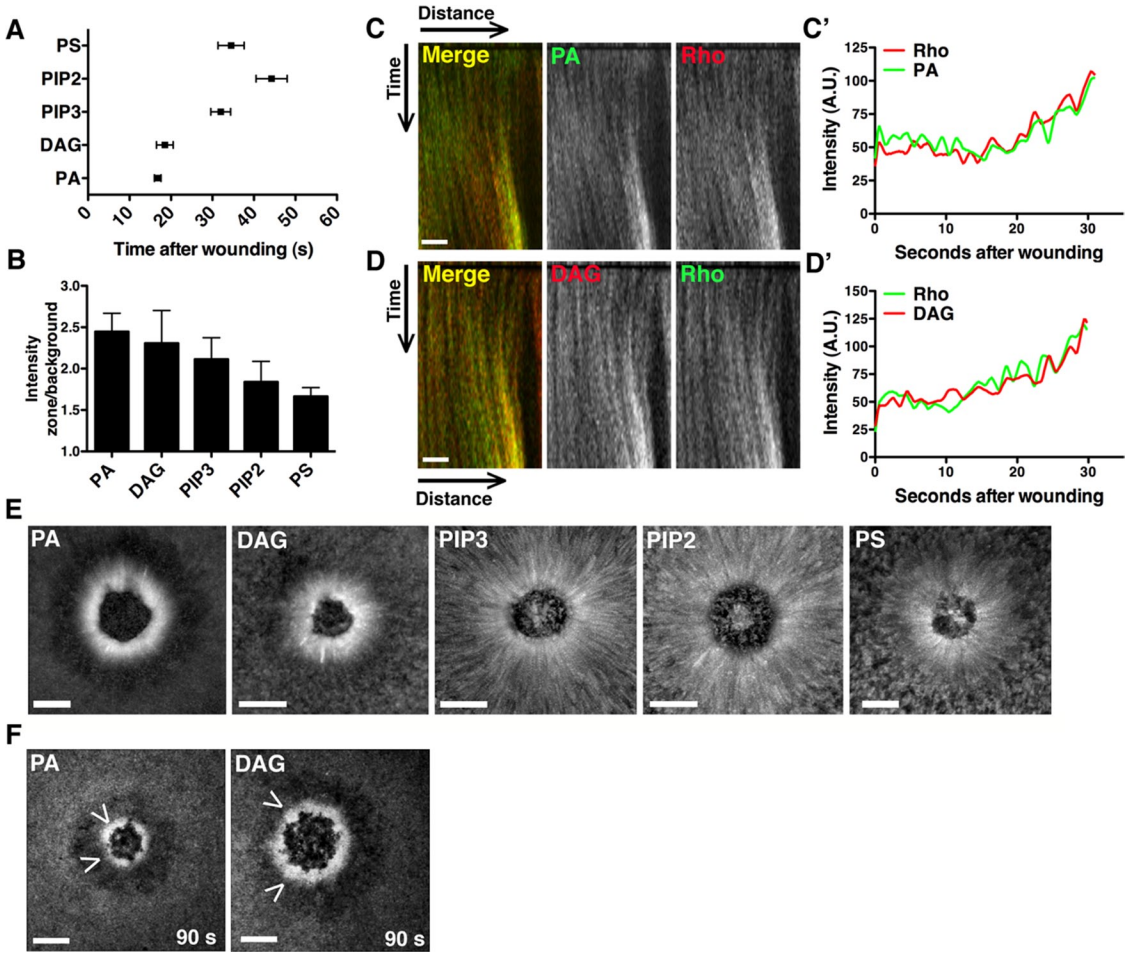

FIGURE 2: PA and DAG are generated at the wound edge coincident with Rho GTPase activation. (A) Recruitment times for each lipid were quantified. PA appeared at 16.8 s, and DAG at 18.5 s, whereas PIP3, PIP2, and PS accumulated at ≥32 s (PA, $n = 10$; DAG, $n = 12$; PIP3, $n = 12$; PIP2, $n = 8$; PS, $n = 8$; error bars, SEM). (B) The ratio of zone/background fluorescence intensity was calculated for each lipid at 90 s (PA, PIP3, $n = 6$; DAG, PIP2, PS, $n = 5$; error bars, SEM). (C) Cells injected with mCherry-rGBD and eGFP-Spo20 were wounded. A kymograph shows corecruitment of active Rho and PA to the wound edge. (C′) The intensity/time plotted from a vertical line drawn through the wound edge in C. (D) Cells injected with eGFP-rGBD and mRFP-C1 were wounded. A kymograph shows corecruitment of active Rho and DAG to the wound edge. (D′) Intensity/time plotted from a vertical line drawn through the wound edge in D. (E) Brightest-point projections from movies show the contribution of cortical flow (indicated by lines perpendicular to the wound edge) to enrichment of each lipid. PA and DAG are less dependent on cortical flow than PIP3, PIP2, and PS. (F) Cells were treated with latrunculin A to abolish actin-mediated cortical flow, but PA and DAG still accumulated, as indicated by arrowheads. Scale bar, 10 μm (C, D); 20 μm (E, F).

fluorescence intensity in the region of the lipid domains around wounds (Figure 3, B–B′ and D–D′), suggesting that DAG generation is PA independent. Similarly, DAG generation was not dependent on PIP2, as treatment with the PI-PLC inhibitor U-73122 (Smith *et al.*, 1990) did not inhibit, but instead increased, DAG at wounds (Figure 3, C–C′). In contrast, D609, a PC-PLC and SMS inhibitor (Amtmann, 1996; Luberto and Hannun, 1998) significantly reduced DAG generation at the wound edge (Figure 3, A–A′), indicating that PC and/or ceramide, rather than PA or PIP2, are sources of DAG during cell damage.

The two major sources of signaling PA are PC (via PLD activity) and DAG (via DAG kinase activity; Wang *et al.*, 2006; Figure 3H). To determine the origin of PA at the wound, we treated cells with the PLD inhibitor FIPI, the DAG kinase inhibitor R59949 (de Chaffoy de Courcelles *et al.*, 1989), or the PC-PLC and SMS inhibitor D609. Treatment with either D609 or R59949 reduced but did not completely eliminate wound-induced PA synthesis (Figure 3, E–E′ and G–G′). In contrast, treatment with FIPI resulted in near-complete inhibition of PA generation after wounding (Figure 3, F–F′). These results suggest that PA is primarily derived from PC, with DAG also partially contributing to the PA enrichment zone at wounds.

DAG is required for Rho and Cdc42 activation

Given that PA and DAG are generated at the proper time and place to activate the Rho GTPases, we explored their potential role in Rho GTPase activation. Treatment with D609, which dramatically reduced DAG and modestly reduced PA at wounds (see foregoing discussion), strongly suppressed Cdc42 and Rho activation (Figure 4, A–C) and led to little apparent wound closure in the first 2 min after wounding. These results implied that DAG, PA, or both might be required for Rho activation. To determine whether PA was

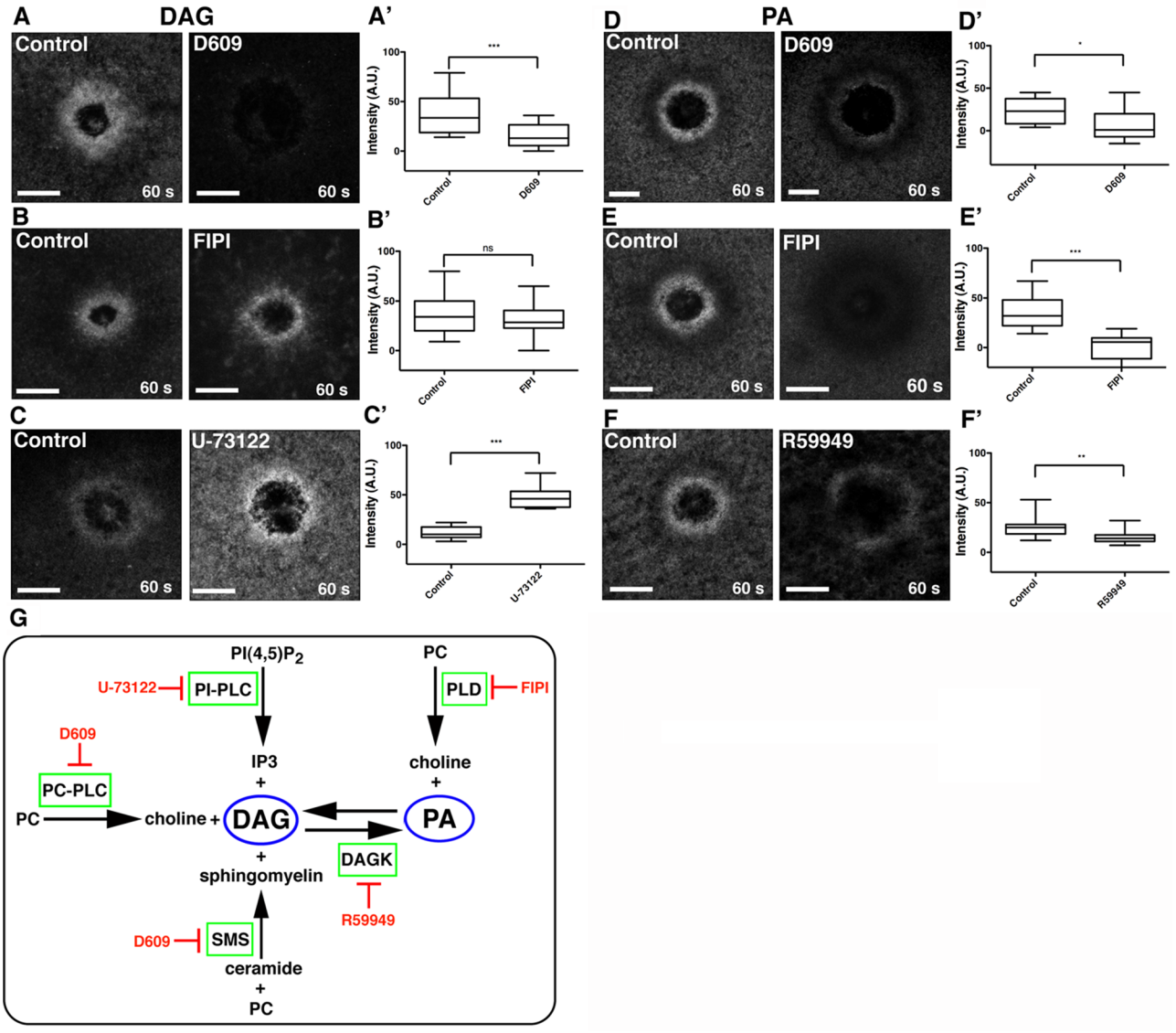

FIGURE 3: DAG is generated via the PC-PLC/SMS pathway, whereas PA is generated via PLD and DAG kinase. (A) DAG is present at wounds in control cells but blocked by the PC-PLC/SMS inhibitor D609. (A′) Quantification of wound DAG (***$p < 0.005$). (B) DAG is present at similar levels at wounds in control cells and those treated with FIPI, a PLD inhibitor. (B′) Quantification of wound DAG ($p > 0.05$). (C) DAG at wounds is elevated in cells treated with the PIP2-PLC inhibitor U-73122. (C′) Quantification of wound DAG (***$p < 0.005$). (D) PA is decreased in cells treated with D609 relative to controls. (D′) Quantification of wound PA (*$p < 0.05$). (E) PA wound signal is blocked in cells treated with FIPI. (E′) Quantification of wound PA (***$p < 0.005$). (F) PA levels at wounds are decreased in cells treated with R59949, a DAG kinase inhibitor. (F′) Quantification of wound PA (**$p < 0.01$). (G) Schematic of pathways leading to DAG and PA generation and corresponding inhibitors. Top and bottom whiskers represent maximum and minimum values, respectively. Scale bar, 20 μm.

responsible for this phenotype, we treated cells with FIPI to reduce PA levels independently of DAG. However, FIPI treatment had no significant effect on Rho activation and stimulated Cdc42 activation in response to wounding (Figure 4, A and C), showing that DAG, rather than PA, is essential for Rho and Cdc42 activation after wounding. Further, treatment with U-73122, which up-regulates DAG (see earlier discussion), also increases levels of active Rho and active Cdc42 (Supplemental Figure S2, A and C), whereas propranolol, which does not affect DAG levels, did not affect Rho and Cdc42 (Supplemental Figure S2, B and D).

To further assess the role of DAG in the wound response, we sought a second means to inhibit PC-PLC. Unfortunately, no eukaryotic PC-PLC has been identified, precluding knockdown or dominant-negative approaches. We therefore tested SPK-601, a putative PC-PLC inhibitor (Walker, 2010). Because SPK-601 is being developed as a potential therapeutic, information concerning its effective range is proprietary. We therefore directly assayed SPK-601 as a PC-PLC inhibitor using PC-PLC purified from *Bacillus cereus* (see *Materials and Methods*). SPK-601 inhibited PC-PLC in vitro, with a dose–response curve and IC_{50} similar to those of D609 (Figure 5A). Further, in agreement with the data obtained with D609, SPK-601 also inhibited production of DAG and PA in vivo in response to wounding (Figure 5B), as well as of the activation of Rho and Cdc42 around wounds (Figure 5C).

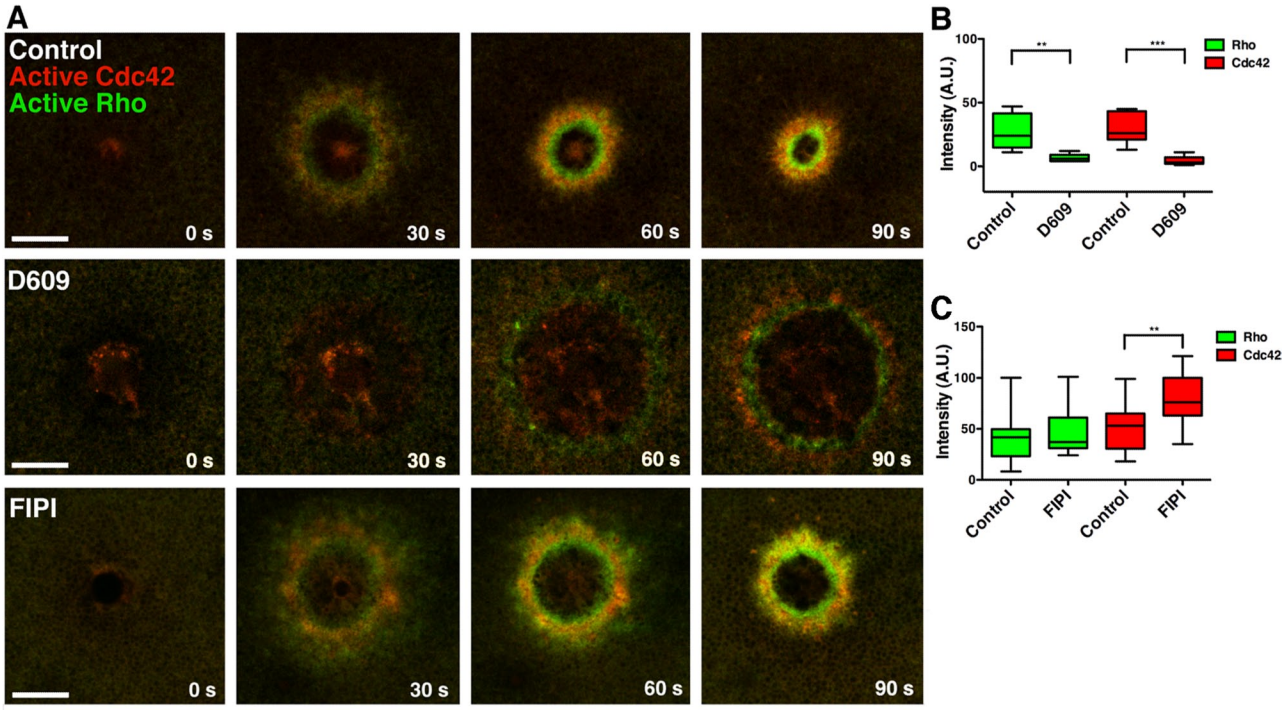

FIGURE 4: Blocking generation of DAG, but not PA, inhibits Rho and Cdc42 activation. (A) Cells were injected with eGFP-rGBD and mRFP-wGBD to detect active Rho and active Cdc42, respectively. In cells treated with D609, Rho and Cdc42 activity is inhibited and wound healing stalls, whereas FIPI treatment does not inhibit GTPase activity or healing. (B) Intensity of Rho and Cdc42 zones from control and D609-treated cells was quantified at 60 s (Rho: control vs. D609, $p < 0.01$; Cdc42: control vs. D609, $p < 0.005$). (C) Intensity of Rho and Cdc42 zones from control and FIPI-treated cells was quantified at 60 s (Rho: control vs. FIPI, $p > 0.05$; Cdc42: control vs. FIPI, $p < 0.01$). Top and bottom whiskers represent maximum and minimum values, respectively. Scale bar, 20 μm.

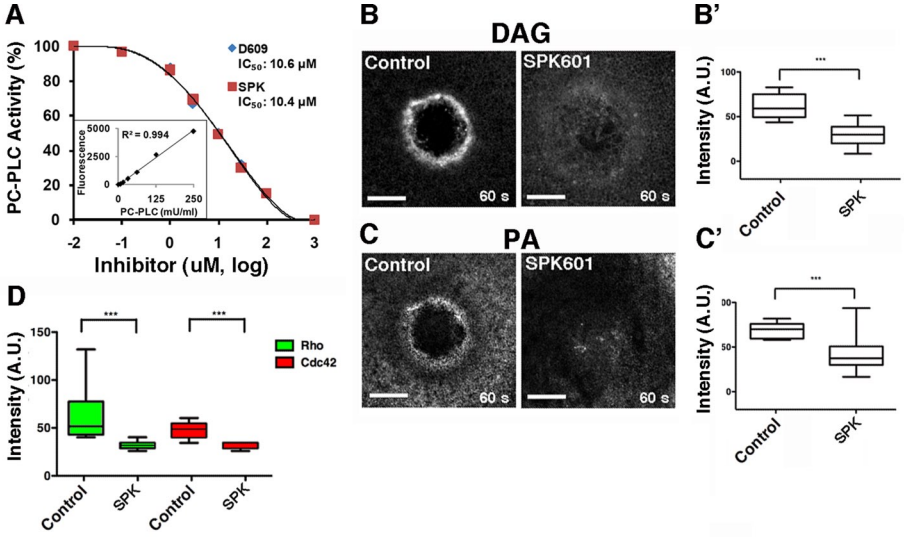

FIGURE 5: SPK601 inhibits PC-PLC, DAG production, and Rho and Cdc42 activation. (A) SPK601 (SPK) is as an effective inhibitor of PC-PLC in vitro as D609. Lipase activity of purified PC-PLC was assayed at the indicated concentrations of each inhibitor. (B) SPK601 suppresses DAG production around wounds. (B') Quantification of wound DAG ($p < 0.005$). (C) SPK601 suppresses PA production around wounds. (C') Quantification of wound PA ($p < 0.005$). (D) SPK601 suppresses Rho and Cdc42 activation around wounds. Intensity of Rho and Cdc42 zones from control and SPK601-treated cells was quantified at 60 s (Rho: control vs. SPK601, $p < 0.005$; Cdc42: control vs. SPK601, $p < 0.005$). Top and bottom whiskers represent maximum and minimum values, respectively. Scale bar, 20 μm.

DAG is required for healing

The foregoing results indicate that suppression of DAG generation reduces healing over the course of the first few minutes after wounding. To determine whether suppression of DAG production affects healing of single cell wounds over a longer time course, we used the stab wound assay (Clark *et al.*, 2012). In this assay, oocytes are stab wounded with glass needles in the presence of putative inhibitors or dimethyl sulfoxide (DMSO), the vehicle, and then allowed to heal overnight. Cells that heal successfully are intact to the following day; those that do not, lyse. At concentrations sufficient to suppress DAG production in vivo, both SPK-601 and D609 sharply impaired healing in this assay relative to the DMSO controls (Figure 6A). Neither of these agents, however, caused lysis after overnight treatment in the absence of wounding, even when applied at 400 μM (unpublished data). Of importance, significant healing failure was evident at the same concentrations required to significantly suppress production of DAG around wounds (Figure 6B).

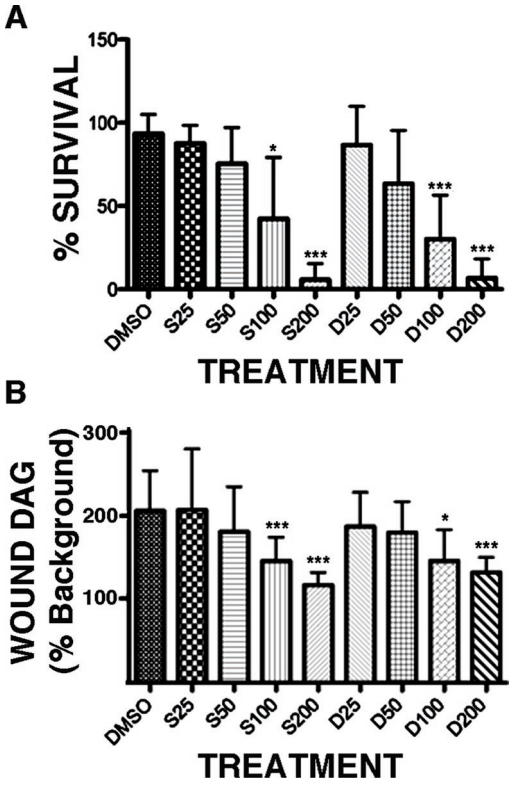

FIGURE 6: Dose-dependent suppression of healing and DAG production by SPK601 or D609. (A) Cells were treated with DMSO, the vehicle, or the indicated micromolar concentrations of SPK601 (S) or D609 (D) for 1 h, stab wounded with a glass needle, cultured overnight, and then assessed for survival. SPK601 and D609 both significantly suppressed healing at concentrations of 100 or 200 µM. (B) Quantification of wound DAG levels in cells treated as in A. Bars, mean ± SD; *$p < 0.05$; ***$p < 0.005$.

PKCβ and PKCη differentially regulate Rho and Cdc42 zones

On the basis of the foregoing results, on previous studies indicating that the PKCs—well-known DAG targets—participate in the single-cell wound response (Bement and Capco, 1991; Togo *et al.*, 1999), and on evidence that the PKCs participate in Rho GTPase activation in *Xenopus* eggs (Yu and Bement, 2007), we investigated the localization of different *Xenopus* PKCs after wounding. PKCβ, a conventional PKC regulated by binding to calcium and DAG (Newton, 1997), is rapidly recruited to a region that encompasses both the Rho (unpublished data) and the Cdc42 zones (Figure 7A and Supplemental Figure S3, A–A′). PKCη and δ, novel PKCs regulated by DAG but not calcium binding, are also rapidly recruited to wounds but in a much narrower domain, corresponding to the region of DAG synthesis (Figure 7A and Supplemental Figure S3, B–B′ and C–C′). In contrast, PKCλ, which does not bind DAG, fails to localize to wounds (Supplemental Figure S3D). Further, inhibition of DAG generation with D609 significantly reduces the localization of PKCη and PKCβ to the wound (Supplemental Figure S3, E and F). Thus DAG-dependent PKC isoforms are rapidly targeted to wounds in a DAG-dependent manner.

Potential roles for the PKCs in the wound response were assessed by overexpressing PKCβ or PKCη or expressing dominant-negative (DN) versions of these proteins. PKCβ overexpression significantly upregulated wound-induced Rho and Cdc42 activation, whereas expression of DN PKCβ significantly down-regulated Rho and Cdc42 activation (Figure 7, C– E). In contrast, overexpression of PKCη inhibited Rho and Cdc42 activation (Figure 7, C and F), as did overexpression of PKCδ (Supplemental Figure S3G). Curiously, in ~20% of the cells overexpressing PKCη, the reduced Rho zone was displaced outside the Cdc42 zone (Supplemental Figure S3H). In keeping with its apparent role as an inhibitor of Rho and Cdc42, expression of DN PKCη significantly up-regulated Rho and Cdc42 activation at the cortex (Figure 7, C and G). These results suggest that PKCβ positively regulates the Rho GTPases, whereas PKCη and δ negatively regulate them. Consistent with this notion, simultaneous overexpression of PKCη and expression of DN PKCβ almost completely suppressed Rho and Cdc42 activation in response to wounding (Figure 5, C and H). Thus two different classes of PKC—conventional and novel—play apparently antagonistic roles in wound repair.

DISCUSSION

The results presented here provide what is, to the best of our knowledge, the first demonstration of a role for a specific lipid—DAG—in the single-cell wound response. DAG may function indirectly by signaling to Rho and Cdc42 (e.g., Yu and Bement, 2007). However, in addition to PKC activation, DAG promotes membrane fusion (e.g., Zick *et al.*, 2014), an obvious means for this lipid to promote the repair response. The concentration of DAG around wounds, as well as its role in the healing response in vivo, suggests that in vitro behavior of putative protein players in the healing process should be analyzed under conditions in which DAG is included in the relevant assays. It also follows from the results that manipulations that increase DAG production or mimic DAG should be considered as potential therapies for pathologies resulting from compromised wound repair.

More generally, the discovery of multiple distinct lipid domains around wounds, each with a characteristic spatial and temporal pattern of accumulation, supports the idea that cells can organize plasma membrane lipids as signaling platforms. However, the diversity of such domains seen here goes far beyond any other example in the literature, and the micrometer scale of the domains greatly exceeds the hypothesized nanometer scale of lipid rafts (Owen *et al.*, 2012). However, our results are consistent with recent work in demonstrating micrometer-scale domains enriched with sphingosine (Frisz *et al.*, 2013a,b; for review, see Kraft, 2013).

Although we focused on DAG in this work, largely due to the timing of its accumulation at wounds, this should not be taken to imply that the other lipids are not involved in the repair process. We think it likely that most or all of them play roles in the developing wound array, although the roles may be subtle. The concentration of acidic phospholipids in the regions overlapping the Rho and Cdc42 zones, for example, may help maintain these zones, in that such lipids are believed to promote the liberation of Rho GTPases from GDP dissociation inhibitor (e.g., Fauré *et al.*, 1999).

In no case did we observe complete recovery of normal plasma membrane lipid distribution within at least 3 min of wounding. This contrasts with the oft-stated expectation that repair of the plasma membrane takes place within seconds of damage but is consistent with recent results obtained using a generic membrane marker in *Drosophila* syncytial embryos (Abreu-Blanco *et al.*, 2011). Thus it might be useful to draw a distinction between the point at which the plasma membrane hole is sealed and the point at which the plasma membrane has completely regenerated. Further, given the recent demonstration that plasma membrane wounds in cultured cells can be open for >1 min (Jimenez *et al.*, 2014), the assumption that resealing occurs within seconds may need to be reevaluated.

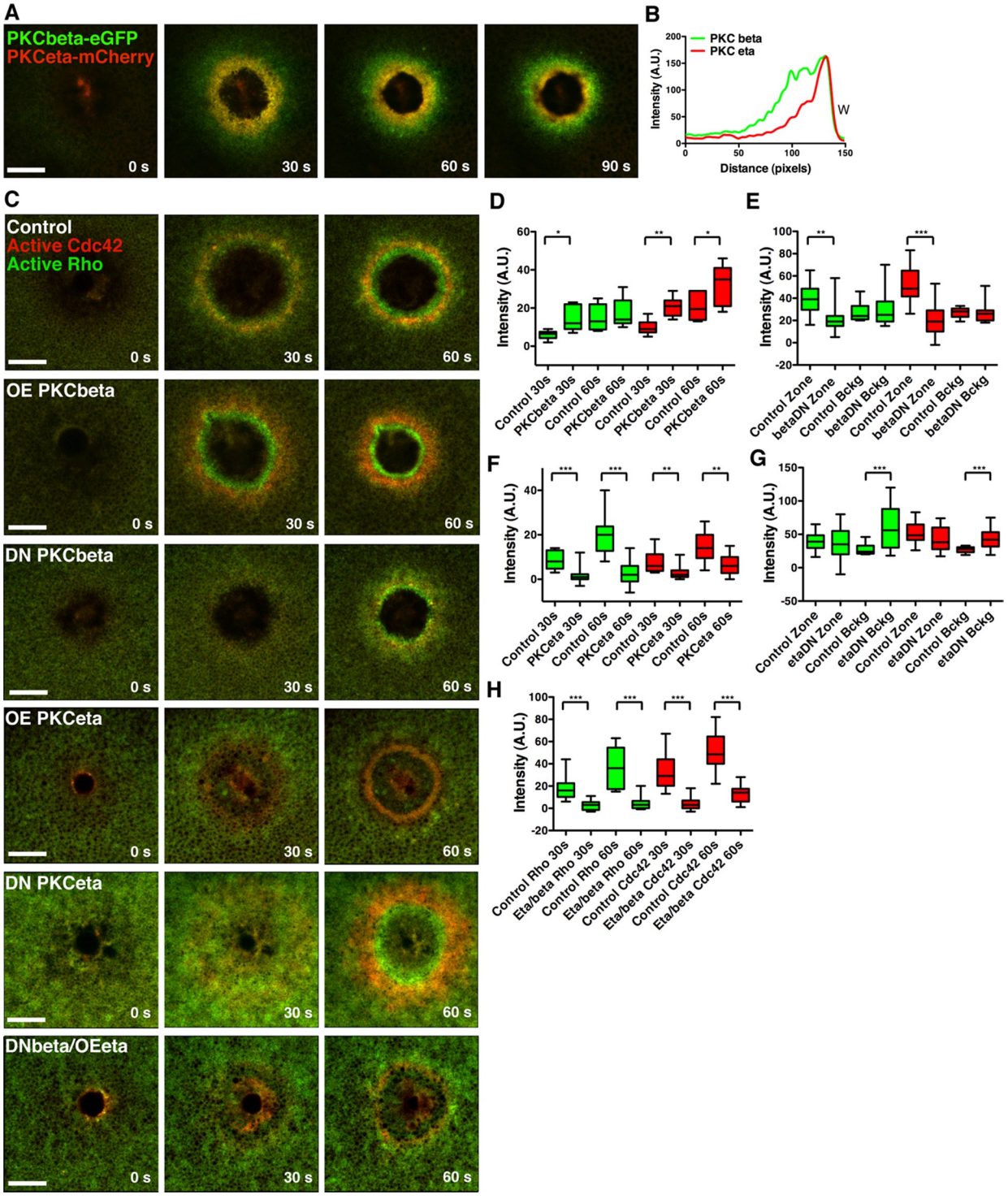

FIGURE 7: PKCβ and PKCη differentially regulate Rho and Cdc42 zones. (A) Cells injected with PKCβ -eGFP and PKCη-mCherry reveal localization of both PKCs to the wound edge, with PKCβ spanning a broader region than PKCη. (B) A line scan from the 90-s time point of A. (C) Cells were injected with eGFP-rGBD and mRFP-wGBD alone or with PKCβ, DN PKCβ, PKCη, DN PKCη, or DN PKCβ and PKCη. PKCβ up-regulates Rho and Cdc42 activity zones, whereas DN PKCβ down-regulates zones. PKCη inhibits Rho and Cdc42 activity zones, whereas DN PKCβ up-regulates Rho and Cdc42 activity on the cortex. Expression of DN PKCβ and full-length PKCη results in dramatic inhibition of both Rho and Cdc42 activity zones. (D) Quantification of Rho and Cdc42 zone intensity at 30 and 60 s with PKCβ expression (control, $n = 6$; PKCβ, $n = 7$). (E) Quantification of Rho and Cdc42 zone intensity at 60 s and background intensity with DN PKCβ expression (control, $n = 16$; PKCβ DN, $n = 11$). (F) Quantification of Rho and Cdc42 zone intensity at 30 and 60 s with PKCη expression ($n = 14$). (G) Quantification of Rho and Cdc42 zone intensity at 60 s and background intensity with DN PKCη expression (control, $n = 16$; PKCη DN, $n = 11$). (H) Quantification of Rho and Cdc42 zone intensity at 30 and 60 s with expression of DN PKCβ and full-length PKCη (control, $n = 16$, PKCβ DN/PKCη, $n = 13$). Green bars, Rho; red bars, Cdc42. Top and bottom whiskers represent maximum and minimum values, respectively. Scale bar, 20 μm. W, wound.

Finally, the results add to the growing body of evidence that the single-cell wound response is far more complex and ordered than originally believed. In the frog oocyte system, for example, results from several different studies point to discrete zones of Rho GTPase activity (Benink and Bement, 2005), regions within zones that differ in terms of cytoskeleton (Mandato and Bement, 2001), Rho GTPase turnover (Burkel *et al.*, 2012), Rho GTPase GEF localization (Vaughan *et al.*, 2011; Simon *et al.*, 2013), and now, additional subdivisions based on differences in lipid and protein kinase C isoform distribution. Nor is this likely to be frog oocyte specific, in that recent work on *Drosophila* embryos suggests that in that model, cellular damage similarly elicits a highly organized series of signaling and cytoskeletal events (Abreu-Blanco *et al.*, 2011, 2014), while other basic features of the cell wound response are conserved in budding yeast (Kono *et al.*, 2012) and mammalian cells (Lin *et al.*, 2012). How does this plasma membrane compartmentalization arise, and what purpose does it serve? With respect to the former, we suspect that it results from hierarchies of interactive gradients initiated by wounding that collaboratively direct the observed compartmentalization (Bement and von Dassow, 2014). With respect to the latter, we think it probable that compartmentalization contributes to the characteristic speed and flexibility of the cellular wound response.

MATERIALS AND METHODS

Plasmids

mRFP-wGBD and enhanced green fluorescent protein (eGFP)–rGBD were made as previously described (Benink and Bement, 2005). Spo20p$^{51\text{-}91}$ was subcloned into pCS2+–eGFP with *Bam*H1 and *Cla*1. eGFP-PKCη C1 and mRFP-PKCη C1 were made by inserting the fragment encoding His167-Cys310 of PKCη with *Bsp*E1 and *Xba*1 into eGFP-pCS2+ or mRFP-pCS2+, respectively. eGFP-PH (GRP1$^{240\text{-}398}$) was obtained from M. Halloran (University of Wisconsin–Madison, Madison, WI) and subcloned into eGFP-pCS2+ or mCherry-pCS2+ with *Bsp*E1 and *Xho*1. eGFP-PH (PLC δ) was obtained from T. Meyer (Stanford University, Stanford, CA) and subcloned into the pCS2+ vector. eGFP-C2 (lactadherin [Lact]) was obtained from Haematologic Technologies (Essex Junction, VT) and subcloned into pCS2-mCherry with *Cla*1 and *Eco*R1. The *Xenopus laevis* PKCβ-pCS2+, PKCβ-eGFP, PKCβ C1-C2 (DN PKCβ), eGFP-PKCβ C1, and eGFP-PKCβ C1^{mut} constructs were made as described (Yu and Bement, 2007). *X. laevis* PKCη (BC073353) was amplified from cDNA and inserted into pCS2+ with *Bam*H1 and *Xho*1 restriction enzymes and into pCS2+–eGFP and pCS2+–mCherry with *Bst*B1 and *Xba*1 restriction enzymes. The DN PKCη C2-C1 construct was created by inserting the region corresponding to amino acids 1–294 of PKCη into pCS2+ with *Bam*H1 and *Xba*1 restriction enzymes. PKCδ (BC078019) was obtained from Open Biosystems, and the coding sequence was inserted into pCS2+ and pCS2+–eGFP with *Stu*1 and *Xba*1. aPKCλ (*Xenopus tropicalis*) was obtained from N. Papalopulu (University of Manchester, Manchester, United Kingdom) and subcloned into pCS2+–eGFP with *Stu*1 and *Xba*1.

Oocyte preparation and injections

Xenopus oocytes were obtained and stored as described (Yu and Bement, 2007). Where plasmid DNA was injected, 20 nl was injected into the nucleus 48 h before imaging. eGFP-C2 (Lact) plasmid was injected at 100 µg/ml, and eGFP-Spo20 and eGFP-Spo20^{mut} were injected at 50 µg/ml. mRNA was transcribed in vitro using mMessage mMachine SP6 kit (Ambion, Grand Island, NY). Oocytes were injected with 40-nl volume of mRNA 24 h before imaging. eGFP-rGBD and mRFP-wGBD were injected at 250 µg/ml needle concentration. Spo20-eGFP was injected at 750 µg/ml. All C1-domain–containing probes were injected at 500 µg/ml. eGFP-PH (GRP1) was injected at 600 µg/ml, and mCherry-PH (GRP1) was injected at 800 µg/ml. eGFP-PH (PLCδ) was injected at 50 µg/ml, and C2 (Lact)-mCherry was injected at 100 µg/ml. PKCβ-eGFP, PKCη-eGFP, and PKCη-mCherry were injected at 500 µg/ml. PKCδ-eGFP and aPKCλ-eGFP were injected at 1 mg/ml. For overexpression, PKCβ was injected at 1.5 mg/ml, and PKCη and PKCδ were both injected at 2 mg/ml. For DN experiments, PKCη C2-C1 and PKCβ C1-C2 mRNAs were polyadenylated using the Poly(A) tailing kit (Ambion) and injected at 2 mg/ml. Alexa Fluor 647–G-actin (Molecular Probes, Grand Island, NY) was diluted to 1 mg/ml in G-Buffer before injection and imaged after 15 min.

Inhibitors

Cells were incubated in 5 µM latrunculin A (Calbiochem, Darmstadt, Germany) for 80–120 min. For experiments with D609 (Calbiochem), oocytes were washed and incubated in 1× Barth's at pH 6.9, with 10 mM 1,4-piperazinediethanesulfonic acid in place of 4-(2-hydroxyethyl)-1-piperazineethanesulfonic acid. From 100 to 200 µM D609 or SPK601 (1% DMSO for control) was added to cells 30–75 min before wounding. FIPI hydrochloride hydrate, 1 µM (Sigma-Aldrich; 0.1% DMSO for control), was added to cells 20–45 min before wounding. U-73122, 1 µM (Calbiochem; 0.1% EtOH for control), was added to cells 5–30 min before wounding. (R)-(±)-Propranolol hydrochloride, 400 µM (Calbiochem; 0.08% MeOH for control), was added to cells 5–10 min before wounding. R59949, 100 µM (Calbiochem; 1% DMSO for control), was added to cells 60–90 min before wounding.

For quantification of D609 and SPK-601 inhibition of PC-PLC in vitro, 150 mU/ml *B. cereus* PC-PLC was purified and preincubated with the inhibitors for 5 min before starting the LIPASE reaction (purchased from Invitrogen). Reactions were run for 60 min in presence of fluorescent PLC substrate, and PLC activity was monitored by measuring fluorescence of the reaction product at 492/520 nm.

For the long-term wounding assay, oocytes were preincubated in the indicated concentrations of SPK-601 or D609 or, as a control, DMSO, for 1 h and then stabbed four times with a 30-µm (tip width) glass needle and incubated overnight at 17°C. Other controls were maintained in 200–400 µM SPK-601 or D609 overnight without wounding. After overnight incubation, oocytes were scored for lysis by inspection with a dissecting microscope (Clark *et al.*, 2012).

Microscopy and data analysis

Four-dimensional imaging experiments were conducted using an Axiovert 100M (Carl Zeiss Microimaging, Thornwood, NY) with the Lasersharp Confocal package (model 1024; Bio-Rad) with a 63× objective. Cells were wounded with a Micropoint pulse nitrogen-pumped dye laser (Laser Science, Mumbai, India). Brightest-point projections, kymographs line scans, and intensity data were obtained using ImageJ software (National Institutes of Health, Bethesda, MD). Brightest-point projections are *z*-projections of maximum-intensity points from three-dimensional movies. Line scans are derived from a 10-pixel-wide line drawn through the wound edge, and lines were smoothened by averaging four neighbor data points and using a second-order polynomial with Prism 5. Distinct lipid domains were characterized by signal peaks ≥1 µm apart. Zone intensity quantifications were obtained as described previously (Vaughan *et al.*, 2011). Data analysis and graphing was conducted with Excel 2004 for Mac (Microsoft) and Prism 5 for Mac OSX. Statistically significant results correspond to the following *p* values: $*p < 0.05$, $**p < 0.01$, $***p < 0.001$.

ACKNOWLEDGMENTS

This work was supported by National Institutes of Health Grant GM52932 to W.M.B. T.A.H. was supported by National Institutes of Health Grant AR057347, and N.V. was supported by Agence Nationale de la Recherche Grant ANR-09-BLAN-0264.

REFERENCES

Abreu-Blanco MT, Verboon JM, Parkhurst SM (2011). Cell wound repair in *Drosophila* occurs through three distinct phases of membrane and cytoskeletal remodeling. J Cell Biol 193, 455–464.

Abreu-Blanco MT, Verboon JM, Parkhurst SM (2014). Coordination of Rho family GTPase activities to orchestrate cytoskeleton responses during cell wound repair. Curr Biol 24, 144–155.

Amtmann E (1996). The antiviral, antitumoural xanthate D609 is a competitive inhibitor of phosphatidylcholine-specific phospholipase C. Drugs Exp Clin Res 22, 287–294.

Bansal D, Miyake K, Vogel SS, Groh S, Chen CC, Williamson R, McNeil PL, Campbell KP (2003). Defective membrane repair in dysferlin-deficient muscular dystrophy. Nature 423, 168–172.

Bement WM, Capco DG (1991). Analysis of inducible contractile rings suggests a role for protein kinase C in embryonic cytokinesis and wound healing. Cell Motil Cytoskeleton 20, 145–157.

Bement WM, von Dassow G (2014). Single cell pattern formation and transient cytoskeletal arrays. Curr Opin Cell Biol 26C, 51–59.

Benink HA, Bement WM (2005). Concentric zones of active RhoA and Cdc42 around single cell wounds. J Cell Biol 168, 429–439.

Burkel BM, Benink HA, Vaughan EM, von Dassow G, Bement WM (2012). A Rho GTPase signal treadmill backs a contractile array. Dev Cell 14, 23384–23396.

Cai C *et al.* (2009). MG53 nucleates assembly of cell membrane repair machinery. Nat Cell Biol 11, 56–64.

Clark AG, Sider JR, Verbrugghe K, Fenteany G, von Dassow G, Bement WM (2012). Identification of small molecule inhibitors of cytokinesis and single cell wound repair. Cytoskeleton 69, 1010–1020.

de Chaffoy de Courcelles D, Roevens P, Van Belle H, Kennis L, Somers Y, De Clerck F (1989). The role of endogenously formed diacylglycerol in the propagation and termination of platelet activation. A biochemical and functional analysis using the novel diacylglycerol kinase inhibitor, R 59 949. J Biol Chem 264, 3274–3285.

Dries DR, Gallegos LL, Newton AC (2007). A single residue in the C1 domain sensitizes novel protein kinase C isoforms to cellular diacylglycerol production. J Biol Chem 282, 826–830.

Fauré J, Vignais PV, Dagher MC (1999). Phosphoinositide-dependent activation of Rho A involves partial opening of the RhoA/Rho-GDI complex. Eur J Biochem 262, 879–889.

Frisz JF *et al.* (2013a). Direct chemical evidence for sphingolipid domains in the plasma membranes of fibroblasts. Proc Natl Acad Sci USA 110, E613–E622.

Frisz JF, Klitzing HA, Lou K, Hutcheon ID, Weber PK, Zimmerberg J, Kraft ML (2013b). Sphingolipid domains in the plasma membranes of fibroblasts are not enriched with cholesterol. J Biol Chem 288, 16855–16861.

Godin LM, Vergen J, Prakash YS, Pagano RE, Hubmayr RD (2011). Spatiotemporal dynamics of actin remodeling and endomembrane trafficking in alveolar epithelial type I cell wound healing. Am J Physiol Lung Cell Mol Physiol 300, L615–L623.

Gray A, Van Der Kaay J, Downes CP (1999). The pleckstrin homology domains of protein kinase B and GRP1 (general receptor for phosphoinositides-1) are sensitive and selective probes for the cellular detection of phosphatidylinositol 3,4-bisphosphate and/or phosphatidylinositol 3,4,5-trisphosphate in vivo. Biochem J 344, 929–936.

Howard AC, McNeil AK, Xiong F, Xiong WC, McNeil PL (2011). A novel cellular defect in diabetes: membrane repair failure. Diabetes 60, 3034–3043.

Jimenez AJ, Maiuri P, Lafaurie-Janvore J, Divoux S, Piel M, Perez F (2014). ESCRT machinery is required for plasma membrane repair. Science 343, 1247136.

Kono K, Saeki Y, Yoshida S, Tanaka K, Pellman D (2012). Proteasomal degradation resolves competition between cell polarization and cellular wound healing. Cell 150, 151–164.

Kraft ML (2013). Plasma membrane organization and function: moving past lipid rafts. Mol Biol Cell 24, 2765–2768.

Lapidos KA, Kakkar R, McNally EM (2004). The dystrophin glycoprotein complex: signaling strength and integrity for the sarcolemma. Circ Res 94, 1023–1031.

Laval SH, Bushby KM (2004). Limb-girdle muscular dystrophies—from genetics to molecular pathology. Neuropathol Appl Neurobiol 30, 91–105.

Lennon NJ, Kho A, Bacskai BJ, Perlmutter SL, Hyman BT, Brown RH Jr (2003). Dysferlin interacts with annexins A1 and A2 and mediates sarcolemmal wound-healing. J Biol Chem 278, 50466–50473.

Lin P, Zhu H, Cai C, Wang X, Cao C, Xiao R, Pan Z, Weisleder N, Takeshima H, Ma J (2012). Nonmuscle myosin IIA facilitates vesicle trafficking for MG53-mediated cell membrane repair. FASEB J 26, 1875–1883.

Liu P, Li RL, Zhang L, Wang QL, Niehaus K, Baluska F, Samaj J, Lin JX (2009). Lipid microdomain polarization is required for NADPH oxidase-dependent ROS signaling in Picea meyeri pollen tube tip growth. Plant J 60, 303–313.

Luberto C, Hannun YA (1998). Sphingomyelin synthase, a potential regulator of intracellular levels of ceramide and diacylglycerol during SV40 transformation. Does sphingomyelin synthase account for the putative phosphatidylcholine-specific phospholipase C? J Biol Chem 273, 14550–14559.

Mandato CA, Bement WM (2001). Contraction and polymerization cooperate to assemble and close actomyosin rings around *Xenopus* oocyte wounds. J Cell Biol 154, 785–797.

McNeil AK, Rescher U, Gerke V, McNeil PL (2006). Requirement for annexin A1 in plasma membrane repair. J Biol Chem 281, 35202–35207.

McNeil PL, Steinhardt RA (2003). Plasma membrane disruption: repair, prevention, adaptation. Annu Rev Cell Dev Biol 19, 697–731.

Mellman I, Nelson WJ (2008). Coordinated protein sorting, targeting and distribution in polarized cells. Nat Rev Mol Cell Biol 9, 833–845.

Newton AC (1997). Regulation of protein kinase C. Curr Opin Cell Biol 9, 161–167.

Owen DM, Magenau A, Williamson D, Gaus K (2012). The lipid raft hypothesis revisited—new insights on raft composition and function from super-resolution fluorescence microscopy. Bioessays 34, 739–747.

Raucher D, Stauffer T, Chen W, Shen K, Guo S, York JD, Sheetz MP, Meyer T (2000). Phosphatidylinositol 4,5-bisphosphate functions as a second messenger that regulates cytoskeleton-plasma membrane adhesion. Cell 100, 221–228.

Simon CM, Vaughan EM, Bement WM, Edelstein-Keshet L (2013). Pattern formation of Rho GTPases in single cell wound healing. Mol Biol Cell 24, 421–432.

Smith RJ, Sam LM, Justen JM, Bundy GL, Bala GA, Bleasdale JE (1990). Receptor-coupled signal transduction in human polymorphonuclear neutrophils: effects of a novel inhibitor of phospholipase C-dependent processes on cell responsiveness. J Pharmacol Exp Ther 253, 688–697.

Sonnemann KJ, Bement WM (2011). Wound repair: toward understanding and integration of single-cell and multicellular wound responses. Annu Rev Cell Dev Biol 27, 237–263.

Su W, Yeku O, Olepu S, Genna A, Park JS, Ren H, Du G, Gelb MH, Morris AJ, Frohman MA (2009). 5-Fluoro-2-indolyl des-chlorohalopemide (FIPI), a phospholipase D pharmacological inhibitor that alters cell spreading and inhibits chemotaxis. Mol Pharmacol 75, 437–446.

Takeda T, Kawate T, Chang F (2004). Organization of a sterol-rich membrane domain by cdc15p during cytokinesis in fission yeast. Nat Cell Biol 6, 1142–1144.

Togo T, Alderton JM, Bi GQ, Steinhardt RA (1999). The mechanism of facilitated cell membrane resealing. J Cell Sci 112, 719–731.

Vaughan EM, Miller AL, Yu HY, Bement WM (2011). Control of local Rho GTPase crosstalk by Abr. Curr Biol 21, 270–277.

Wakelam MJ (1998). Diacylglycerol—when is it an intracellular messenger? Biochim Biophys Acta 1436, 117–126.

Walker K (2010). Interscience Conference on Antimicrobial Agents and Chemotherapy - 50th Annual Meeting - Research on Promising New Agents: Part 1. IDrugs 13, 743–745.

Wang X, Devaiah SP, Zhang W, Welti R (2006). Signaling functions of phosphatidic acid. Prog Lipid Res 45, 250–278.

Yeung T, Gilbert GE, Shi J, Silvius J, Kapus A, Grinstein S (2008). Membrane phosphatidylserine regulates surface charge and protein localization. Science 319, 210–213.

Yu HY, Bement WM (2007). Control of local actin assembly by membrane fusion-dependent compartment mixing. Nat Cell Biol 9, 149–159.

Zeniou-Meyer M *et al.* (2007). Phospholipase D1 production of phosphatidic acid at the plasma membrane promotes exocytosis of large dense-core granules at a late stage. J Biol Chem 282, 21746–21757.

Zick ML, Stroupe C, Orr A, Douville D, Wickner WT (2014). Membranes linked by trans-SNARE complexes require lipids prone to non-bilayer structure for progression to fusion. Elife 3, e01879.